Homochiral Xanthine Quintet Networks Self-Assembled on Au(111) Surfaces

Miao Yu,[†,‡,*] Jianguo Wang,[§] Manuela Mura,[⊥,∥] Qiang-qiang Meng,[§] Wei Xu,[†] Henkjan Gersen,[¶] Erik Lægsgaard,[†] Ivan Stensgaard,[†] Ross E. A. Kelly,[#] Jørgen Kjems,[†] Trolle R. Linderoth,[†] Lev N. Kantorovich,[⊥] and Flemming Besenbacher[†,*]

[†]Interdisciplinary Nanoscience Center (iNANO) and Department of Physics and Astronomy, Aarhus University, 8000 Aarhus C, Denmark, [‡]School of Chemical Engineering and Technology, Harbin Institute of Technology, Harbin 150001, People's Republic of China, [§]Institute of Industrial Catalysis, Zhejiang University of Technology, Hangzhou 310032, People's Republic of China, [⊥]Department of Physics, King's College London, The Strand, London WC2R 2LS, United Kingdom, [∥]University of Central Lancashire, Preston PR1 2HE, United Kingdom, [¶]H.H. Wills Physics Laboratory, University of Bristol, Bristol BS8 1TL, United Kingdom, and [#]Department of Physics and Astronomy, University College London, London WC1E 6BT, United Kingdom

ABSTRACT Xanthine molecule is an intermediate in nucleic acid degradation from the deamination of guanine and is also a compound present in the ancient solar system that is found in high concentrations in extraterrestrial meteorites. The self-assembly of xanthine molecules on inorganic surfaces is therefore of interest for the study of biochemical processes, and it may also be relevant to the fundamental understanding of prebiotic biosynthesis. Using a combination of high-resolution scanning tunneling microscopy (STM) and density functional theory (DFT) calculations, two new homochiral xanthine structures have been found on Au(111) under ultrahigh vacuum conditions. Xanthine molecules are found to be self-assembled into two extended homochiral networks tiled by two types of di-pentamer units and stabilized by intermolecular double hydrogen bonding. Our findings indicate that the deamination of guanine into xanthine leads to a very different base pairing potential and the chemical properties of the base which may be of relevance to the function of the cell and potential development of human diseases. Moreover, the adsorption of xanthine molecules on inorganic surfaces leading to homochiral assemblies may be of interest for the fundamental understanding of the emerged chirality at early stages of life.

KEYWORDS: hydrogen bonding · prebiotic earth · purine · scanning tunneling microscopy · self-assembly

Xanthine molecule (3,7-dihydropurine-2,6-dione, $C_5H_4N_4O_2$, as shown in Figure 1) is an intermediate in nucleic acid degradation from the spontaneous or nitrosative deamination of guanine, where the amine group of guanine is substituted by an oxygen atom in xanthine.[1−3] Xanthine exists in both prokaryote and eukaryote cells and participates in a large variety of functions in most human body tissues and fluids, hence self-assembly of xanthine molecules is of interest for the study of biochemical processes. Furthermore, xanthine is a compound present in the ancient solar system and is found in high concentrations in extraterrestrial meteorites.[4] It has recently been demonstrated that this purine is one of the original exogenous nucleobases abundant in prebiotic age on Earth[4−8] and may have been one of the precursors for nucleic acids.[9] The adsorption of xanthine molecules on inorganic surfaces is therefore of interest for the fundamental understanding of prebiotic biosynthesis[5] and may be of relevance to the origin and evolution of life as well.[7,10−18]

Guanine molecules adsorbed on solid surfaces have been studied extensively under ultrahigh vacuum (UHV), liquid and ambient conditions using scanning tunneling microscopy (STM),[19−22] which makes it possible to reveal the supramolecular architectures with molecular precision. It has been demonstrated that guanine molecules form supramolecular networks tiled in quartets (four-molecule units) which are stabilized by intermolecular hydrogen bonding. Guanine is a prochiral molecule which can be adsorbed in an either face-up or face-down adsorption configuration on the substrates and thus induces a chirality of these quartet structures.[20] However, the adsorption of xanthine molecules on surfaces is much less studied. Only STM and atomic force microscopy (AFM) results of xanthine at a graphite−water interface or on graphite and MoS_2 solid surfaces in air have been reported,[5,23] where two-dimensional (2-D) domains of close-packed chain-like motifs were observed.

In the present work, the adsorption of xanthine has been investigated on Au(111) under well-controlled UHV conditions using a combination of high-resolution STM imaging and state-of-the-art density functional

* Address correspondence to fbe@inano.au.dk, miaoyu_che@hit.edu.cn.

Received for review June 11, 2011 and accepted July 13, 2011.

Published online July 13, 2011
10.1021/nn202157m

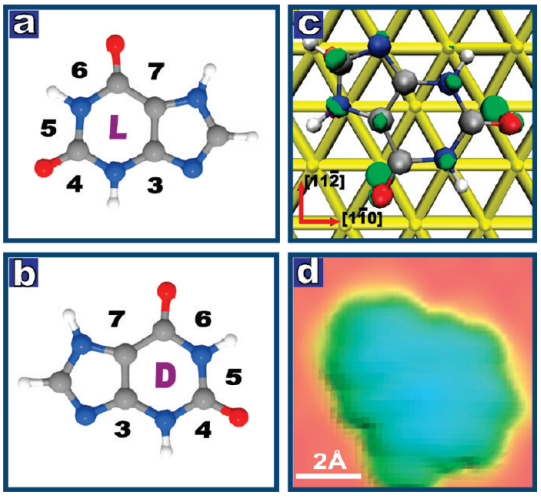

Figure 1. (a) Adsorption-induced left-handed L-chiral and (b) right-handed D-chiral ball/stick models of xanthine, where carbon, hydrogen, oxygen, and nitrogen atoms are shown in gray, white, red, and blue, respectively. Several relevant binding sites of the molecules are numbered for convenience as shown. (c) Calculated charge density difference plot of an individual xanthine adsorbed flat on the Au(111) surface, showing the absence of charge transfer between the surface and the molecule. (d) Simulated STM image of a single xanthine molecule on gold demonstrating its pseudotriangular appearance.

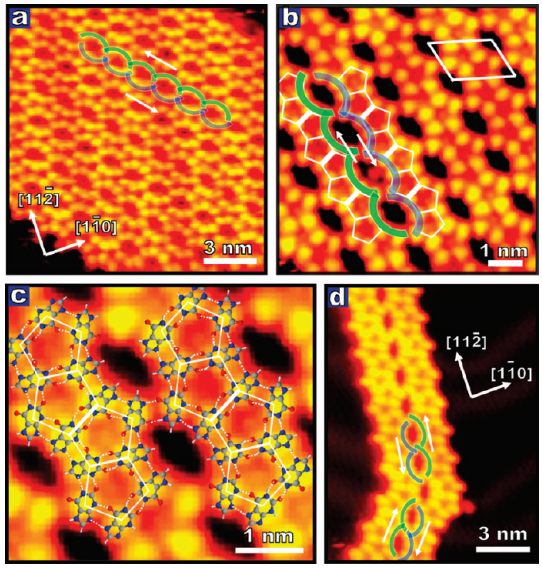

Figure 2. (a) Large-scale STM image of the compact-zigzag (CZ) structure, showing a well-ordered close-packed 2-D domain of zigzag xanthine stripes. (I_t = 0.26 nA, V_t = 1250 mV). (b) Close view showing a formation composed of tiles of di-pentamers in a single orientation, emphasized by the white pentagons (I_t = 0.46 nA, V_t = 884 mV). (c) High-resolution STM image superimposed by the proposed DFT model shown in Figure 5d, revealing that the network is stabilized by inner- and interstripe double hydrogen bonds (I_t = 0.65 nA, V_t = 884 mV). (d) STM image of a bent double-stripe xanthine filament on the Au(111), showing that the CZ domains are developed from zigzag stripes (I_t = 0.30 nA, V_t = 1250 mV).

theory (DFT) calculations. Two new structures of xanthine have been revealed, where xanthine molecules are self-assembled into two highly ordered extended networks tiled by two types of di-pentamer units and stabilized by intermolecular double hydrogen bonding between molecules. Strikingly, it is found that the self-assembled xanthine structures are homochiral, which may have implications for the emerged chirality at early stages of life.

RESULTS AND DISCUSSION

Xanthine is prochiral upon adsorption (see Figure 1a for L-chiral (left-handed) and Figure 1b for D-chiral (right-handed) xanthine), which is similar to guanine. When xanthine is deposited by thermal evaporation onto the Au(111) surface kept at room temperature, each individual molecule adopts a flat-lying geometry, as depicted in Figure 1c. Depending on the deposition coverage, three different adsorption structures are observed: (i) at low coverages of 0.2−0.4 ML (ML = monolayer), two distinct types of extended 2-D networks of xanthine are formed, denoted as *compact-zigzag* (CZ) and *sunflower* structures (shown in Figures 2 and 3, respectively); and (ii) at a coverage of 0.4 ML or higher, large domains of a close-packed chain-like structure are formed (see the Supporting Information). The chain-like structure is consistent with the xanthine structures reported previously[5,23] and is very similar to the high-coverage structure observed for guanine molecules.[19,21,22] This chain-like structure can also coexist with the CZ structure within the same domains (see Supporting Information).

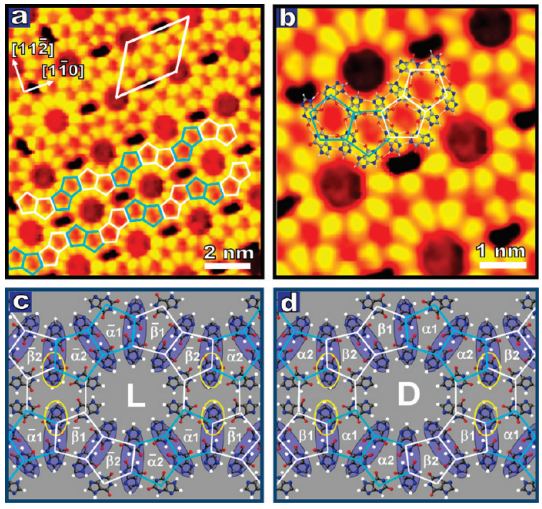

Figure 3. (a) Example of STM images of the sunflower structure (named due to the characteristic 10-molecule circular rings) showing a formation tiled by di-pentamers in two orientations, marked in white and blue pentagons, respectively (I_t = 0.27 nA, V_t = 1250 mV). (b) High-resolution STM image of this xanthine structure with the DFT relaxed structure superimposed (I_t = 0.33 nA, V_t = 1250 mV). (c,d) DFT calculated sunflower networks after full relaxation, composed of L- and D-chiral xanthines, respectively. Dim blue ovals highlight the characteristic 5−5 dimers (see text).

In all cases, each xanthine molecule appears in the STM image as a pseudotriangular feature similar to that of a guanine molecule. This is consistent with the

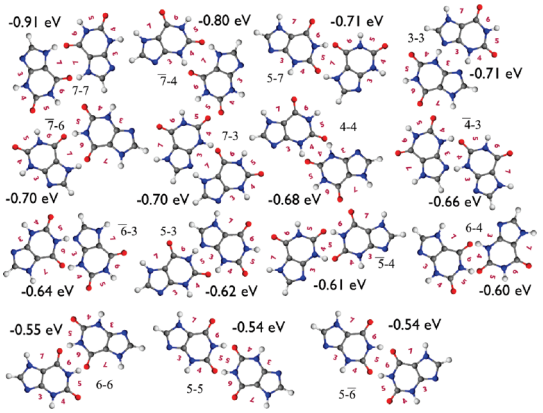

Figure 4. Most stable xanthine dimers and their stabilization energies (without the BSSE) calculated using the DMol package.

calculated STM image of an individual xanthine in Figure 1d using a scattering method (see Supporting Information) and is also in good agreement with previous STM simulations of xanthine on graphite based on total and partial electron density plots.[24] The resultant STM contrast is attributed to the interaction between delocalized π-molecular orbitals of the purine and the metallic electronic density of the Au substrate. The underlying herringbone reconstruction of the Au(111) substrate[25] is still observed as a modulation of the corrugation over xanthine islands for all different structures (*e.g.*, Figure 2a).[26] The charge density difference of an individual xanthine adsorbed flat on the Au(111) surface, depicted in Figure 1c, also indicates that there is no charge transfer between the molecule and surface. The DFT results (to be discussed below) show that a single xanthine molecule is physisorbed on the Au(111) surface predominantly due to van der Waals (vdW) interaction with an adsorption energy of 0.57 eV. This is consistent with earlier experimental and DFT results for other purine molecules such as guanine,[19,20] cytosine,[27,28] and adenine[29,30] on Au(111). To investigate the corrugation of the surface potential for a single xanthine molecule and hence calculate the corresponding diffusion barriers, we placed the molecules at a distance of 3.5 Å above the gold surface (the optimum height calculated with the vdW/DF method for the initial randomly chosen lateral position) and translated it in steps of 0.1 Å along several directions across the surface (see the Supporting Information). These DFT calculations show that the change of the binding energy due to lateral displacement of the molecule is indeed very small (of the order of 0.03 eV), which indicates that xanthine molecules are highly mobile on Au(111) at room temperature. Therefore, the self-assembly of the xanthine networks is predominantly driven by intermolecular interactions rather than by molecule−substrate interactions.

Highly ordered domains of the CZ xanthine structure are depicted in Figure 2a. In the high-resolution STM

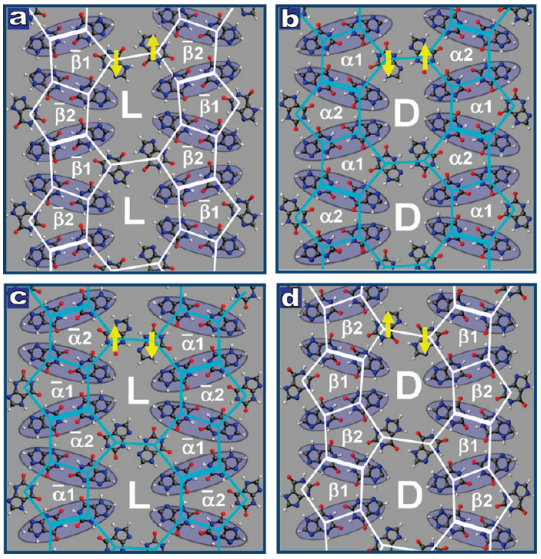

Figure 5. Models relaxed with our DFT method of (a) L-chiral and (b) D-chiral compact-zigzag-1 and (c) L-chiral and (d) D-chiral compact-zigzag-2 structures, where the relative shift of the half rings is indicated by yellow arrows. Each pentagon is marked as explained in the text, with structures composed of α-, $\bar{\alpha}$-stripes and β-, $\bar{\beta}$-stripes colored in pale blue and white, respectively. Note that $\bar{\alpha}$- and $\bar{\beta}$-stripes are mirror images of α- and β-stripes, respectively.

image (Figure 2b), the unit cell is indicated with dimensions of $(1.4 \pm 0.1) \times (2.0 \pm 0.2)$ nm^2 and the acute angle of $63 \pm 2°$. Very interestingly, we find that the network is tiled by xanthine di-pentamers in a single orientation composed of 8 molecules each. The di-pentamer units are indicated by the white twin pentagons in Figure 2b, with the borderline of two neighboring di-pentamers emphasized by thick white lines. This is clearly different from the assembly of guanine molecules on Au(111), in which case the basic building block consists of square-like guanine quartets composed of 4 molecules.[19,20,22,31,32] Black oval-shaped pores are formed between the neighboring zigzag stripes of xanthine as marked on the STM images. It is noticed that these CZ structures are not reflection symmetric. Two different configurations exist, referred to as CZ-1 (Figure 2a,d) and CZ-2 (Figure 2b,c) and distinguished by the relative positions of neighboring stripes, depicted by the white arrows and half ovals in blue and green, respectively. For CZ-1, the left half oval is downshifted relative to its right half, whereas for CZ-2, it behaves oppositely. Two configurations are found to coexist in the same domain, for example, as in the bent filament in Figure 2d, where the CZ-1 structure above the inflection transfers into the CZ-2 structure below it. The ability of xanthine molecular stripes to bend is similar to that of, for example, cytosine filaments.[28] Some insight into the formation kinetics of this striped structure is also revealed in Figure 2d; that is, xanthine molecules are first stabilized into

zigzag stripes and further packed sideways *via* intermolecular hydrogen bonding into extended islands.

Out of 14 tautomeric conformations of xanthine molecules formed through either keto−enol transformation or proton exchange in the ring containing nitrogen atoms,[33,34] all models investigated in our extended DFT calculations are based on the most stable xanthine tautomer (see Supporting Information). The stability of xanthine dimers has been investigated by connecting two molecules with each other *via* binding sites shown in Figure 1 in all possible ways. The most stable dimers and their binding energies (without BSSE correction[35]) are shown in Figure 4. The dimers of the same chirality are labeled by the pair of binding sites which they are connected with, for example, a 5−5 dimer composed of two molecules linked with each other *via* the common site 5. If one of the dimers is flipped, it is shown by a bar above the site number (*e.g.*, $\overline{7}$−6). Dimers 7−7, 7−5, 3−7, 3−3, 3−5, and 5−5 were also calculated using the SIESTA code,[36] resulting in stabilization energies of −0.87, −0.70, −0.66, −0.64, −0.57, and −0.51 eV, respectively. The BSSE correction varies between 0.15 and 0.21 eV. Note that the results of the SIESTA calculations are very close to those of the DMol package[37,38] reported in Figure 4. It is found that the most stable dimer is the 7−7 one, whereas the other homochiral dimers found in the compact-zigzag structure (and also in the sunflower one; see below) are less stable. The 7−3, 5−7, and 3−3 dimers are less stable by about 0.2 eV, while the dimers 5−3 and 5−5 are even less stable. Note that besides the homochiral dimers, there are also heterochiral dimers with high stabilization energies (*e.g.*, $\overline{7}$−4), as seen in Figure 4. This point is essential for our further discussion on chirality of the observed assemblies.

The DFT calculations reveal four different optimized models for the CZ structure depicted in Figure 5, although only two types of structures could be distinguished in our STM images. The models in Figure 5 with the right half of each ring shifted upward relative to its left half are consistent with the experimentally observed CZ-1 structure shown in Figure 2a,d. They are composed of either L- or D-chiral xanthine molecules, respectively, referred to as L-CZ-$\overline{\beta}$ (Figure 5a) and D-CZ-α (Figure 5b). The models with the opposite shift of the rings are consistent with the CZ-2 structure of Figure 2b,c, referred to as L-CZ-$\overline{\alpha}$ (Figure 5c) and D-CZ-β (Figure 5d) for the two different chiralities, respectively. (The definition of α, β, $\overline{\alpha}$, and $\overline{\beta}$ is addressed in the text below.)

In all of these structures, each xanthine molecule is connected with its three neighbors *via* double hydrogen bonds, resulting in very stable configurations. The interstripe hydrogen bonding is facilitated by shared molecules *via* either double N−H···O (Figure 5a,d) or double N−H···N (Figure 5b,c) hydrogen bonds. On the basis of a significant number of structures investigated in our DFT calculations, we conclude that if all molecules involved are kept to be three-fold coordinated to their nearest neighbors by double hydrogen bonding to achieve the most stable formation, only the *homochiral* networks fit the xanthine molecular arrangement obtained experimentally. Note from the calculations that the domains of L-chiral structures of the CZ structure can coexist with the D-chiral ones on the surface. If each of the CZ structures of D-xanthine is flipped, it results in a mirror image composed of L-chirality xanthine: the D-CZ-α (Figure 5b) gives rise to L-CZ-$\overline{\alpha}$ (Figure 5c) and D-CZ-β (Figure 5d) to L-CZ-$\overline{\beta}$ (Figure 5a). The relaxed cell dimensions for models in Figure 5a,d and Figure 5b,c are 1.7 × 2.2 nm^2 and 1.7

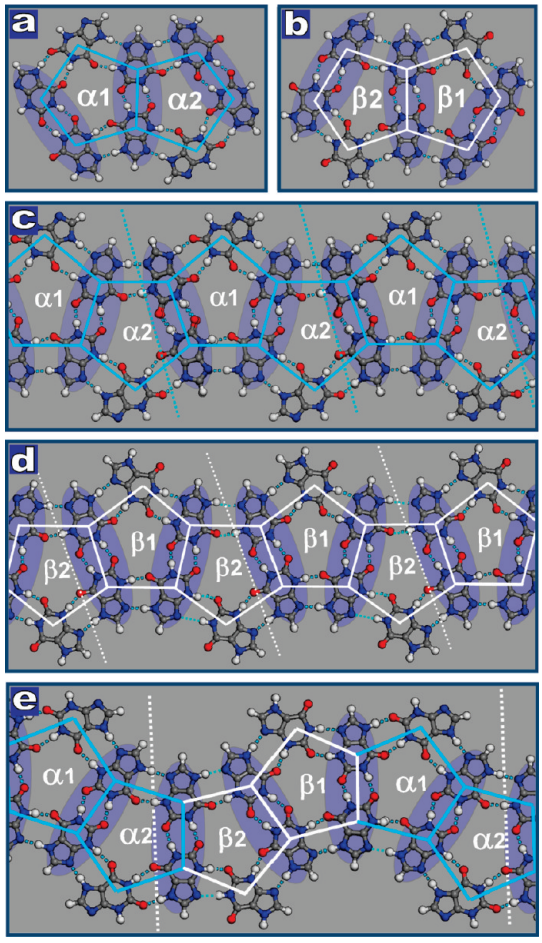

Figure 6. (a) Di-pentamer-α and (b) di-pentamer-β serve as building blocks for the compact-zigzag and sunflower structures. One-dimensional (c) α- and (d) β-stripes composed of the di-pentamer-α and di-pentamer-β, respectively. (e) One-dimensional stripe for the sunflower structure composed of both di-pentamers following one another. Types of the pentamers (α1, α2, β1, and β2) are also indicated in each case. The primitive unit cells in all cases are separated by dashed lines (c−e). All structures correspond to D-chirality and were obtained by our DFT calculations.

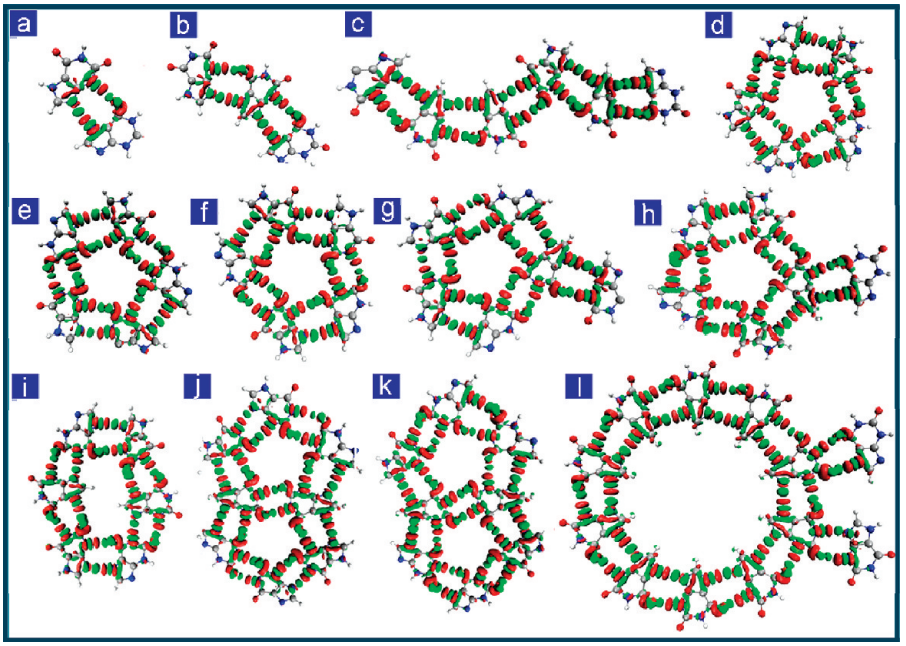

Figure 7. Geometries and density difference plots of a number of xanthine clusters with (a) two (dimer 3−7), (b) three, (c,g−i) six, (d−f) five, (j,k) eight, and (l) 12 molecules. The density plots correspond to isosurfaces of ±0.01e/Å^3 with the green surfaces corresponding to regions of positive electron density difference (excess) and the red areas to regions of negative electron density difference (depletion).

× 2.3 nm^2, and the acute angles are 63 and 64°, respectively, which are both in a very good agreement with the experimental cell dimensions.

According to our DFT calculations, each CZ structure consists of unit cells with 6 molecules and can be considered as one-dimensional (1-D) zigzag stripe compositions. It is sufficient to consider the D-chiral models only, shown in Figure 6c,d, as L-models are obtained simply by reflection. When parallel stripes are brought together, 2-D self-assembled structures are formed. One can see that both stripes consist of an identical zigzag assembly formed by the particular pair of xanthine molecules bound to each other *via* sites 5 (see Figure 1a,b). This particular 5−5 dimer is indicated by the dim blue oval in Figure 6, as well as in Figures 3 and 5. Additional molecules are placed in the spaces between the blue ovals, and two such molecules exist in each unit cell. In fact, the particular orientation of these two molecules is what makes the α- and β-stripes (as depicted in Figure 6c,d) different. This is also why the D-CZ-α (Figure 5b) and D-CZ-β structures (Figure 5d) are different. The two stripes can be regarded as being tiled by di-pentamer-α and di-pentamer-β units (see Figure 6a,b), respectively, which in turn consist of pentagons α1, α2, and β1, β2. So, a single zigzag stripe of the D-CZ-α structure consists of the pentagon sequence ...-α1-α2-α1-α2-..., while the sequence ...-β1-β2-β1-β2... is characteristic of any stripe in the D-CZ-β structure. Hence, the L-chiral pentamer units in a flipped conformation are denoted as $\overline{\alpha}$1, $\overline{\alpha}$2 and $\overline{\beta}$1, $\overline{\beta}$2.

In Figure 3a,b, STM images for the sunflower structure (named so due to the characteristic 10-molecule circular rings) are depicted. Each unit cell (marked by the white rhombus) is composed of 12 molecules with the dimensions of (3.0 ± 0.2) × (2.7 ± 0.2) nm^2 and the acute angle of 57 ± 1°. Interestingly, it is noticeable that the network is also tiled by di-pentamer units, but in two orientations (marked in white and blue). Each unit is also composed of 8 molecules with 2 molecules shared between neighboring units as in the CZ structures. DFT models for the sunflower structure are depicted in Figure 3c,d. Different from the CZ structure, both the di-pentamer-α and di-pentamer-β units are involved in this sunflower structure. Similarly to the CZ structure, the most stable configuration here is also formed by the *homochiral* xanthine structures. The model in Figure 3c is composed of only L-xanthines, while the mirror-image structure in Figure 3d is formed by D-chiral molecules and obtained by flipping the former structure. It should be stressed that we are not able from STM images to distinguish between these L- and D-chiral structures. In Figure 3b, we have superimposed the D-chiral calculated model with a calculated unit cell of the dimension 3.2 × 2.8 nm^2 and the acute angle of 56°, on the STM image, and the calculated model is in excellent agreement with the experimental results. Twelve xanthine molecules exist in each unit cell: 10 are involved in the sunflower ring structure and two molecules serve as "connectors" between rings, emphasized by yellow ellipses. As in the CZ structure, each xanthine molecule including the connectors is coordinated with its three nearest neighbors interacting *via* double hydrogen bonds. Within the ring, each xanthine molecule interacts with the

TABLE 1. Stabilization, Interaction, Deformation, BSSE, and Per Molecule Stabilization Energies (in eV) for All Considered Clusters: Each Column Corresponds to the Structure Shown in Figure 7

	(a)	(b)	(c)	(d)	(e)	(f)	(g)	(h)	(i)	(j)	(k)	(l)
E_{stab}	−0.66	−1.25	−3.06	−2.84	−2.68	−2.67	−3.36	−3.80	−3.66	−5.00	−5.17	−7.52
E_{bsse}	0.17	0.36	0.93	0.95	0.92	0.91	1.11	0.80	1.16	1.67	1.74	2.24
E_{def}	0.07	0.15	0.36	0.28	0.33	0.34	0.38	0.38	0.41	0.59	0.64	0.86
E_{int}	−0.73	−1.40	−3.42	−3.13	−3.00	−3.01	−3.74	−4.18	−4.12	−5.59	−5.82	−8.38
E_{mol}	−0.33	−0.42	−0.51	−0.57	−0.54	−0.53	−0.56	−0.63	−0.61	−0.62	−0.65	−0.63

TABLE 2. Stabilization, Interaction, Deformation, BSSE, and Per Molecule Energies (in eV) of the Extended Periodic Models

	compact-zigzag-1	compact-zigzag-2	sunflower
E_{stab}	−6.03	−5.85	−11.8
E_{bsse}	1.67	1.65	3.35
E_{def}	1.38	1.21	2.58
E_{int}	−7.41	−7.06	−14.39
E_{mol}	−1.01	−0.96	−0.98

neighboring two ring molecules in the same way as in the CZ structure showing N−H···O bonds in the outer and the N−H···N bond in the inner rings. One can also regard this sunflower structure as packed by *parallel* 1-D stripes of zigzagged identical 5−5 xanthine dimers, as depicted in Figure 6e. One can recognize the same di-pentamer-α and di-pentamer-β building blocks as in the CZ structure but tiling alternatively the entire stripe *via* an infinite sequence ...-(β2-β1)-(α1-α2)-(β2-β1)-... of pentamers.

To understand in greater detail the formation of these particular xanthine structures by the di-pentamers and in order to examine their stability, a large set of different xanthine 2-D clusters and assemblies with various numbers of molecules were calculated using our DFT approach. We calculated formation energies (per molecule) for a fairly large number of planar clusters of xanthine molecules and compared them with the corresponding energies for the extended CZ and sunflower structures. For direct comparison, all calculated structures were relaxed with either DMol or SIESTA method. Although numerous structures have been relaxed using the DMol package, including various pentamers and hexamers, only the SIESTA results (which include the BSSE correction) are given below to demonstrate the general trends. The geometries of the considered xanthine clusters are shown in Figure 7. For each system, we present a number of useful energies in Table 1: E_{stab}, the total stabilization energy; E_{def}, the deformation energy characterizing the energy loss all molecules experience, as compared to the isolated molecules when combined in the actual system; E_{int}, the interaction energy calculated as the total energy of the whole cluster minus energies of all constituent molecules in the geometry of the combined system. The stabilization energy is exactly equal to the sum of the latter two energies. We also present in each case the stabilization energies per molecule, E_{mol}, to facilitate a direct comparison between the different structures.

In addition, in order to characterize the strength of the hydrogen bonding between molecules in any of the gas-phase structures, the electron density difference is shown, which is obtained by subtracting the electron densities of every isolated molecule in the structure from the density of the latter. These plots present "kebab" structures between molecules of alternating regions of depletion and excess of the electron density, characteristic for the hydrogen bonding.[33] In all cases, the kebab structures are well-developed, demonstrating strong double hydrogen bonds between any two molecules, as confirmed by the high stabilization energies shown in Table 1. As the number of hydrogen bonds per molecule increases, so does the per molecule stabilization energy for the different clusters in Figure 7: (a) a dimer has only 2 bonds; (b) a trimer has 4; (c) the di-trimer has 10 hydrogen bonds; (d−f) the pentamers have 10, as well; (g,h) these structures contain 12 bonds in total; one of the molecules is fully saturated, that is, is three-coordinated; (i) this hexamer also contains 12 bonds, however, neither of the molecules is fully saturated; (j,k) these di-pentamers have 18 bonds and two fully saturated molecules; (l) this element of the sunflower structure contains 24 bonds with two molecules being fully saturated, as in the previous two cases. It is revealed that in the larger clusters the possibility of hydrogen bonding is increased, leading to the increase of the stabilization energy per molecule.

Clearly, the extended self-assembled CZ and sunflower structures consisting of all three-fold coordinated molecules are expected to be more stable than the finite xanthine clusters because in either of these two structures the binding of each molecule with neighbors is fully saturated *via* strong double N−H···O and N−H···N hydrogen bonding. To confirm this, the stabilization and other relevant energies of extended compact-zigzag and sunflower structures were calculated by SIESTA method. The SIESTA results are shown in Table 2, which are consistent with the results based on the DMol code. The stabilization energies (per molecule) are found to be close to

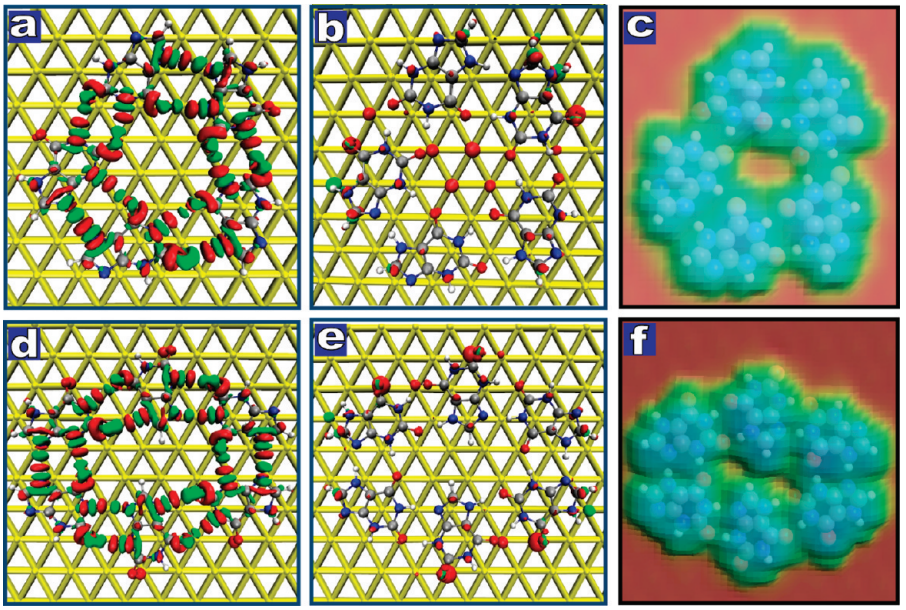

Figure 8. Electron density difference plots of (a,b) the pentamer (as shown in Figure 7d) and (d,e) the hexamer (as shown in Figure 7i) calculated using (a,d) model A (at ±0.01 electrons/Å^3) and (b,e) model B (at ±0.006 electrons/Å^3), respectively. The green surfaces correspond to the regions of positive electron density difference (excess), and the red areas correspond to the regions of negative electrons density difference (depletion). The calculated STM images of (c) the pentamer and (f) the hexamer are both consistent with experimental results.

1.0 eV, and as expected, they are significantly larger than the similar stabilization energies calculated for the xanthine clusters above. This is because every xanthine molecule in either of the periodic structures is fully coordinated; that is, the hydrogen bonds are fully saturated in the considered monolayers. Moreover, we find that the stabilization energies per xanthine molecule in each structure are very close (around 0.67 eV). For this reason and also because either structure is composed of a similar number of hydrogen bonds between the molecules, the probability to form of any of these homochiral structural domains on the surface are most likely identical.

The building blocks of the two extended structures, that is, the xanthine pentamers and the hexamer adsorbed on the Au(111) substrate, have also been studied theoretically by our DFT SIESTA method on the Au(111) substrate to provide direct comparison with experimental STM images. In all cases, these xanthine clusters were first relaxed in the gas phase, then placed on the Au(111) surface and relaxed again using the vdW/DF method. Two methods have been adopted to characterize the electron density of the clusters on the gold surface. (i) Method A: between the complete system (molecules + gold surface) on the one hand and all the individual parts (individual molecules and the gold slab) on the other. (ii) Method B: a similar approach is considered, however, instead of the individual molecules, their gas-phase clusters are considered as a whole. Method A is useful to visualize the hydrogen bonding between molecules *on the surface*, while method B clearly reveals the interaction of the cluster with the surface ignoring the redistribution of the density between molecules due to the hydrogen bonding between them. The density difference plots using both methods for one of the three pentamers (as shown in Figure 7d) and the hexamer (as shown in Figure 7i) in the actual relaxed geometries on the gold surface are shown in Figure 8a,b and 8d,e, respectively. We notice that in all cases the kebab structures for the xanthine clusters on the gold surface (Figure 8a,d) are very similar to those in the gas phase shown in Figure 7d,i. Also, the plots due to method B clearly reveal that there is no charge transfer between the xanthine molecules and the surface. These results are consistent with the expected physisorption character of the binding of the molecules to the surface, which is predominantly due to the vdW interaction as mentioned above. Calculated STM images of the pentamer and the hexamer are depicted in Figure 8c,f, which are both in good agreement with experimental STM results. Similar results for the other two pentamers placed on the gold surface are given in Supporting Information.

In fact, we find that the sunflower and CZ structures can not only coexist on the surface in different domains as described above but also combine with each other within the same island, as depicted in Figure 9a,b. The atomistic models explaining these intricate possibilities, that is, of how these two structures can be connected with each other, are suggested in Figure 9c,d. Remarkably, the chirality of xanthine molecules is preserved across each of these mixed structures.

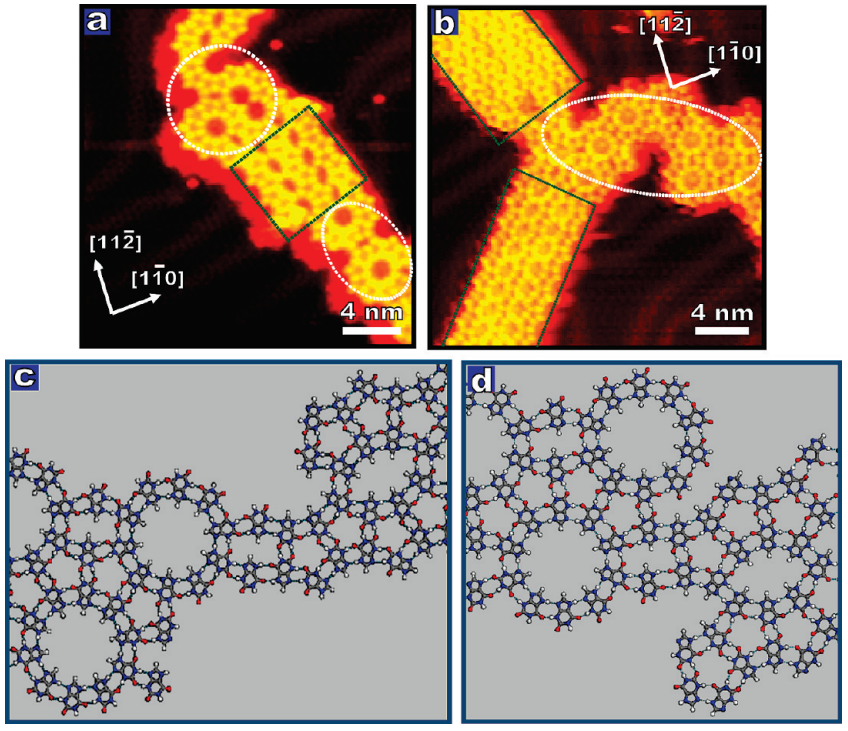

Figure 9. STM images showing a combination of the sunflower structure (marked in white dashed ellipse) and the compact-zigzag structure (emphasized by dark green rectangles). (a) I_t = 0.28 nA, V_t = 1250 mV; (b) I_t = 0.24 nA, V_t = 1250 mV. (c,d) Atomistic models showing examples of two possible connections between the sunflower and compact-zigzag structures.

A detailed analysis reveals that the sunflower and CZ structures, on the whole, do not consist of the most stable dimers. In particular, the 5−5 dimer (see Figure 4) highlighted by a dim blue oval in Figure 5 is over 0.3 eV less stable than the most stable 7−7 dimer, whose only single occurrence (per unit cell) can be found in the D-CZ-β and L-CZ-$\overline{\beta}$ structures. The most frequent dimer structure 3−7 in all three assemblies is approximately 0.2 eV less stable than the 7−7 dimer. Although one can envisage that the most stable dimers 7−7 would be formed first upon deposition of xanthine molecules at room temperature, apparently upon the subsequent annealing, these dimers would break up and others would form, leading to the formation of CZ and sunflower structures as well as the corresponding mixed structures. This rearrangement is facilitated by the high mobility of the molecules (see Supporting Information). Due to the huge number of possibilities, it is not possible to prove that the observed structures are the most energetically favorable. However, we speculate that in these structures an overall balance is established; if structures were based on the most stable dimers like 7−7, this would need to involve many much weaker connections, leading eventually to the less favorable assemblies with overall smaller binding energies (per molecule).

The adsorption-induced chirality of the xanthine molecule may from the first sight resemble that of guanine, where L- and D-guanine molecules form homochiral structures on the Au(111) surface upon evaporation at room temperature.[19,20] However, in the case of guanine, upon annealing a heterochiral structure composed of both L- (left-handed) and R- (right-handed) chiral quartets of guanine can be formed.[20] Since in the present case of xanthine it is not possible to identify any heterochiral xanthine structural models of comparable stability, which would agree with the observed homochiral structures, we conclude that formation of homochiral domains is strongly favored in xanthine assemblies on the Au(111) surface.

CONCLUSIONS

We have demonstrated that, under well-controlled UHV conditions, the xanthine molecules can be self-assembled on the Au(111) surfaces into two distinct structures tiled by two types of di-pentamers. Therefore, the deamination of guanine into xanthine can result in decomposition of the guanine quartet structure, leading to a totally different periodicity, packing, and symmetry of the resultant structures. Furthermore, we have shown that the extended xanthine self-assembled structures are homochiral and that all molecules are three-fold coordinated to nearest neighbors by intermolecular double hydrogen bonding.

It is well-known that environmental toxins, radiation, or endogenous products can directly damage DNA bases *in vivo* by spontaneous and nitrosative deamination,[1−3] resulting in mutagenesis upon repair of affected DNA, which may cause cellular defects implicated in a number of human diseases.[34−36] Our

findings therefore indicate that the deamination of guanine into xanthine leads to a very different base pairing and the chemical properties of the base. Replication of xanthine-containing DNA template most frequently leads to T misincorporation, which will lead to a G to A mutation in the genome,[37] and it may disrupt the guanine quartet structures formed by the telomere sequences at the termini of chromosomes. In the RNA, functionally important secondary and tertiary structures may be disrupted, leading to nonfunctional ribonucleic complexes. Hence, base pairing properties of xanthine play a very important role for the function of the cell and potential development of human diseases.

More importantly, since xanthine is a purine which may have existed in early Earth as a raw extraterrestrial source, our findings may suggest that the adsorption of xanthine on a simple inorganic grain surface may have resulted in the formation of homochiral self-assembled networks at early stages of life, which might potentially have served as precursors for oligonucleotide synthesis. Similar networks may have formed on montmorillonite clay where the extended patches of homochiral xanthine would have ensured a high local concentration of homochiral nucleobases known to undergo oligomerization under these conditions.[13,38] Further studies on adsorption of organic molecules at clay surfaces carried out at ambient conditions are in progress.

METHODS

All experiments were performed in a UHV chamber with a typical base pressure of 1×10^{-10} Torr and equipped with a variable-temperature Aarhus STM[39] as well as facilities for single-crystal sample preparation. The Au(111) single-crystal sample was cleaned by repeated cycles of 1.5 keV Ar^+ ion bombardment and annealing to 850 K for 15 min. Xanthine in powder form was purchased from Sigma-Aldrich and deposited following a thorough degass procedure from a thermal evaporator held at 400 K onto the clean Au(111) sample kept at 300 K. A postannealing of the sample at 350 K for 10 min was then applied. All STM data presented here were collected in the constant current mode in a temperature range of 110−150 K, and an electrochemically etched polycrystalline W tip was used.

For most of the gas-phase systems, the first-principles DFT calculations were performed using the DMol module in Materials Studio.[40,41] The generalized gradient approximation with the PW91 density functional and a high-quality numerical basis set were used. Separate calculations on a single molecule, various pentamers and hexamers adsorbed on the Au(111) surface were performed using the SIESTA method,[42] also implementing a localized basis set. In these calculations, the vdW/DF density functional was used,[26,43,44] which takes self-consistently into account the vdW interaction between the molecules and the surface. The basis set superposition error (BSSE) correction has been calculated in all cases considered with SIESTA using the counterpoise correction method.[45] These calculations revealed relatively strong binding of the molecules to the surface with negligible lateral corrugation rendering molecules to be very mobile at room temperature. This fact also justifies the gas-phase models we adopted for verifying supramolecular assemblies. The STM images were calculated using the Nt_STM code (NANOTIMES) based on the scattering method.[46]

More detailed information on the methods used and the discussion of the results are given in Supporting Information.

Acknowledgment. We gratefully acknowledge the financial support to iNANO from the Danish Research Councils from the Carlsberg Foundation. F.B. acknowledges the European Research Council for an Advanced Grant; H.G. acknowledges the Biotechnology and Biological Sciences Research Council through a Technology Development Research Initiative (Grant BB/F004494/1); J.G.W. acknowledges the National Natural Science Foundation of China (NO. 20906081); and M.M. would like to thank for the computer time allocation on the HECToR U. K. National facilities *via* the Material Chemistry consortium, and the financial support from the EPSRC (Grant No. GR/S97521/01).

Supporting Information Available: The supporting materials of this study are composed of three parts: (1) experimental results on the high-coverage close-packed phase of xanthine on Au(111); (2) theoretical gas-phase calculations, including computational method and calculated stability of xanthine tautomers; (3) calculations of xanthine molecules on the Au(111) surface, including computational method, and results of a single xanthine and xanthine clusters on the Au(111) surface. This material is available free of charge *via* the Internet at http://pubs.acs.org.

REFERENCES AND NOTES

1. Gould, E. S. *Mechanism and Structure in Organic Chemistry*; Holt, Rinehart and Winston: New York, 1959.
2. Singer, B.; Grunberger, D. *Molecular Biology of Mutagens and Carcinogens*; Plenum Press: New York, 1983.
3. Carey, F. A.; Sundberg, R. J. *Advanced Organic Chemistry Part A: Structure and Mechanisms*; Plenum Press: New York, 1990.
4. Martins, Z.; Botta, O.; Fogel, M. L.; Sephton, M. A.; Glavin, D. P.; Watson, J. S.; Dworkin, J. P.; Schwartz, A. W.; Ehrenfreund, P. Extraterrestrial Nucleobases in the Murchison Meteorite. *Earth Planet. Sci. Lett.* **2008**, *270*, 130–136.
5. Sowerby, S. J.; Petersen, G. B. Scanning Tunnelling Microscopy and Molecular Modelling of Xanthine Monolayers Self-Assembled at the Solid−Liquid Interface: Relevance to the Origin of Life. *Origins Life Evol. Biospheres* **1999**, *29*, 597–614.
6. Ferris, J. P.; Hagan, W. J. Hcn and Chemical Evolution: The Possible Role of Cyano Compounds in Prebiotic Synthesis. *Tetrahedron* **1984**, *40*, 1093–1120.
7. Sowerby, S. J.; Cohn, C. A.; Heckl, W. M.; Holm, N. G. Differential Adsorption of Nucleic Acid Bases: Relevance to the Origin of Life. *Proc. Natl. Acad. Sci. U.S.A.* **2001**, *98*, 820–822.
8. Vandervelden, W.; Schwartz, A. W. Search for Purines and Pyrimidines in Murchison Meteorite. *Geochim. Cosmochim. Acta* **1977**, *41*, 961–968.
9. Wachtershauser, G. An All-Purine Precursor of Nucleic-Acids. *Proc. Natl. Acad. Sci. U.S.A.* **1988**, *85*, 1134–1135.
10. Bernal, J. D. *The Physical Basis of Life*; Routledge and Paul: London, 1951.
11. Ertem, G.; Ferris, J. P. Synthesis of RNA Oligomers on Heterogeneous Templates. *Nature* **1996**, *379*, 238–240.
12. Ertem, G.; Ferris, J. P. Template-Directed Synthesis Using the Heterogeneous Templates Produced by Montmorillonite Catalysis. A Possible Bridge between the Prebiotic and RNA Worlds. *J. Am. Chem. Soc.* **1997**, *119*, 7197–7201.
13. Ferris, J. P.; Ertem, G. Oligomerization of Ribonucleotides on Montmorillonite—Reaction of the 5′-Phosphorimidazolide of Adenosine. *Science* **1992**, *257*, 1387–1389.

14. Ferris, J. P.; Hill, A. R.; Liu, R. H.; Orgel, L. E. Synthesis of Long Prebiotic Oligomers on Mineral Surfaces. *Nature* **1996**, *381*, 59–61.
15. Hanczyc, M. M.; Fujikawa, S. M.; Szostak, J. W. Experimental Models of Primitive Cellular Compartments: Encapsulation, Growth, and Division. *Science* **2003**, *302*, 618–622.
16. Hill, A. R.; Bohler, C.; Orgel, L. E. Polymerization on the Rocks: Negatively-Charged α-Amino Acids. *Origins Life Evol. Biospheres* **1998**, *28*, 235–243.
17. Winter, D.; Zubay, G. Binding of Adenine and Adenine-Related Compounds to the Clay Montmorillonite and the Mineral Hydroxylapatite. *Origins Life Evol. Biospheres* **1995**, *25*, 61–81.
18. Otero, R.; Xu, W.; Lukas, M.; Kelly, R. E. A.; Laegsgaard, E.; Stensgaard, I.; Kjems, J.; Kantorovich, L. N.; Besenbacher, F. Specificity of Watson–Crick Base Pairing on a Solid Surface Studied at the Atomic Scale. *Angew. Chem., Int. Ed.* **2008**, *47*, 9673–9676.
19. Otero, R.; Schock, M.; Molina, L. M.; Laegsgaard, E.; Stensgaard, I.; Hammer, B.; Besenbacher, F. Guanine Quartet Networks Stabilized by Cooperative Hydrogen Bonds. *Angew. Chem., Int. Ed.* **2005**, *44*, 2270–2275.
20. Xu, W.; Kelly, R. E. A.; Gersen, H.; Laegsgaard, E.; Stensgaard, I.; Kantorovich, L. N.; Besenbacher, F. Prochiral Guanine Adsorption on Au(111): An Entropy-Stabilized Intermixed Guanine-Quartet Chiral Structure. *Small* **2009**, *5*, 1952–1956.
21. Sowerby, S. J.; Edelwirth, M.; Heckl, W. M. Self-Assembly at the Prebiotic Solid–Liquid Interface: Structures of Self-Assembled Monolayers of Adenine and Guanine Bases Formed on Inorganic Surfaces. *J. Phys. Chem. B* **1998**, *102*, 5914–5922.
22. Heckl, W. M.; Smith, D. P. E.; Binnig, G.; Klagges, H.; Hansch, T. W.; Maddocks, J. 2-Dimensional Ordering of the DNA-Base Guanine Observed by Scanning Tunneling Microscopy. *Proc. Natl. Acad. Sci. U.S.A.* **1991**, *88*, 8003–8005.
23. Tao, N. J.; Shi, Z. Real-Time STM AFM Study of Electron-Transfer Reactions of an Organic-Molecule—Xanthine at the Graphite Water Interface. *Surf. Sci.* **1994**, *321*, L149–L156.
24. Jung, D.; Seo, D. K.; Ren, J.; Whangbo, M. H. Simulation of the Scanning Tunneling and Atomic Force Microscopy Images of a Xanthine Monolayer on Graphite. *Surf. Sci.* **1998**, *401*, 476–481.
25. Barth, J. V.; Brune, H.; Ertl, G.; Behm, R. J. Scanning Tunneling Microscopy Observations on the Reconstructed Au(111) Surface—Atomic-Structure, Long-Range Superstructure, Rotational Domains, and Surface-Defects. *Phys. Rev. B* **1990**, *42*, 9307–9318.
26. Mura, M.; Gulans, A.; Thonhauser, T.; Kantorovich, L. Role of Van der Waals Interaction in Forming Molecule–Metal Junctions: Flat Organic Molecules on the Au(111) Surface. *Phys. Chem. Chem. Phys.* **2010**, *12*, 4759–4767.
27. Kelly, R. E. A.; Lukas, M.; Kantorovich, L. N.; Otero, R.; Xu, W.; Mura, M.; Laegsgaard, E.; Stensgaard, I.; Besenbacher, F. Understanding the Disorder of the DNA Base Cytosine on the Au(111) Surface. *J. Chem. Phys.* **2008**, *129*, 184707.
28. Otero, R.; Lukas, M.; Kelly, R. E. A.; Xu, W.; Laegsgaard, E.; Stensgaard, I.; Kantorovich, L. N.; Besenbacher, F. Elementary Structural Motifs in a Random Network of Cytosine Adsorbed on a Gold(111). *Surf. Sci.* **2008**, *319*, 312–315.
29. Chen, Q.; Frankel, D. J.; Richardson, N. V. Self-Assembly of Adenine on Cu(110) Surfaces. *Langmuir* **2002**, *18*, 3219–3225.
30. Lukas, M.; Kelly, R. E. A.; Kantorovich, L. N.; Otero, R.; Xu, W.; Laegsgaard, E.; Stensgaard, I.; Besenbacher, F. Adenine Monolayers on the Au(111) Surface: Structure Identification by Scanning Tunneling Microscopy Experiment and *Ab Initio* Calculations. *J. Chem. Phys.* **2009**, *130*, 024705.
31. Parkinson, G. N.; Lee, M. P. H.; Neidle, S. Crystal Structure of Parallel Quadruplexes from Human Telomeric DNA. *Nature* **2002**, *417*, 876–880.
32. Smith, F. W.; Feigon, J. Quadruplex Structure of Oxytricha Telomeric DNA Oligonucleotides. *Nature* **1992**, *356*, 164–168.
33. Kelly, R. E. A.; Kantorovich, L. N. Planar Nucleic Acid Base Super-Structures. *J. Mater. Chem.* **2006**, *16*, 1894–1905.
34. Hollstein, M.; Sidransky, D.; Vogelstein, B.; Harris, C. C. P53 Mutations in Human Cancers. *Science* **1991**, *253*, 49–53.
35. Goate, A.; Chartierharlin, M. C.; Mullan, M.; Brown, J.; Crawford, F.; Fidani, L.; Giuffra, L.; Haynes, A.; Irving, N.; James, L. Segregation of a Missense Mutation in the Amyloid Precursor Protein Gene with Familial Alzheimers-Disease. *Nature* **1991**, *349*, 704–706.
36. David, S. S.; O'Shea, V. L.; Kundu, S. Base-Excision Repair of Oxidative DNA Damage. *Nature* **2007**, *447*, 941–950.
37. Eritja, R.; Kaplan, B. E.; Mhaskar, D.; Sowers, L. C.; Petruska, J.; Goodman, M. F. Synthesis and Properties of Defined DNA Oligomers Containing Base Mispairs Involving 2-Aminopurine. *Nucleic Acids Res.* **1986**, *14*, 5869–5884.
38. Joshi, P. C.; Aldersley, M. F.; Delano, J. W.; Ferris, J. P. Mechanism of Montmorillonite Catalysis in the Formation of RNA Oligomers. *J. Am. Chem. Soc.* **2009**, *131*, 13369–13374.
39. Laegsgaard, E.; Osterlund, L.; Thostrup, P.; Rasmussen, P. B.; Stensgaard, I.; Besenbacher, F. A High-Pressure Scanning Tunneling Microscope. *Rev. Sci. Instrum.* **2001**, *72*, 3537–3542.
40. Delley, B. An All-Electron Numerical-Method for Solving the Local Density Functional for Polyatomic-Molecules. *J. Chem. Phys.* **1990**, *92*, 508–517.
41. Delley, B. From Molecules to Solids with the DMol(3) Approach. *J. Chem. Phys.* **2000**, *113*, 7756–7764.
42. Soler, J. M.; Artacho, E.; Gale, J. D.; Garcia, A.; Junquera, J.; Ordejon, P.; Sanchez-Portal, D. The SIESTA Method for *Ab Initio* Order-N Materials Simulation. *J. Phys.: Condens. Matter* **2002**, *14*, 2745–2779.
43. Gulans, A.; Puska, M. J.; Nieminen, R. M. Linear-Scaling Self-Consistent Implementation of The Van der Waals Density Functional. *Phys. Rev. B* **2009**, *79*, 114110.
44. Langreth, D. C.; Lundqvist, B. I.; Chakarova-Kack, S. D.; Cooper, V. R.; Dion, M.; Hyldgaard, P.; Kelkkanen, A.; Kleis, J.; Kong, L. Z.; Li, S. A Density Functional for Sparse Matter. *J. Phys.: Condens. Matter* **2009**, *21*, 084203.
45. Boys, S. F.; Bernardi, F. Calculation of Small Molecular Interactions by Differences of Separate Total Energies: Some Procedures with Reduced Errors. *Mol. Phys.* **1970**, *19*, 553–566.
46. Cerda, J.; Van Hove, M. A.; Sautet, P.; Salmeron, M. Efficient Method for the Simulation of STM Images. I. Generalized Green-Function Formalism. *Phys. Rev. B* **1997**, *56*, 15885–15899.